ACS OMEGA

http://pubs.acs.org/journal/acsodf

Article

Design and Synthesis of Thiazole Scaffold-Based Small Molecules as Anticancer Agents Targeting the Human Lactate Dehydrogenase A Enzyme

Dolly Sharma, Mamta Singh, Jayadev Joshi, Manoj Garg, Vidhi Chaudhary, Daniel Blankenberg, Sudhir Chandna, Vinit Kumar,* and Reshma Rani*

Cite This: *ACS Omega* 2023, 8, 17552−17562

Read Online

ACCESS | Metrics & More | Article Recommendations | Supporting Information

ABSTRACT: A new series of thiazole central scaffold-based small molecules of *h*LDHA inhibitors were designed using an *in silico* approach. Molecular docking analysis of designed molecules with *h*LDHA (PDB ID: 1I10) demonstrates that Ala 29, Val 30, Arg 98, Gln 99, Gly 96, and Thr 94 possessed strong interaction with the compounds. Compounds **8a**, **8b**, and **8d** showed good binding affinity (−8.1 to −8.8 kcal/mol), whereas an additional interaction of NO_2 at the ortho position in compounds **8c** with Gln 99 through hydrogen bonding enhanced the affinity to −9.8 kcal/mol. Selected high-scored compounds were synthesized and screened for *h*LDHA inhibitory activities and *in vitro* anticancer activity in six cancer cell lines. Biochemical enzyme inhibition assays showed the highest *h*LDHA inhibitory activity observed with compounds **8b**, **8c**, and **8l**. Compounds **8b**, **8c**, **8j**, **8l**, and **8m** depicted significant anticancer activities, exhibiting IC_{50} values in the range of 1.65−8.60 μM in HeLa and SiHa cervical cancer cell lines. Compounds **8j** and **8m** exhibited notable anticancer activity with IC_{50} values of 7.90 and 5.15 μM, respectively, in liver cancer cells (HepG2). Interestingly, compounds **8j** and **8m** did not induce noticeable toxicity in the human embryonic kidney cells (HEK293). *In silico* absorption, distribution, metabolism, and excretion profiling demonstrates that the compounds possess drug-likeness, and results may pave the way for the development of novel thiazole-based biologically active small molecules for therapeutics.

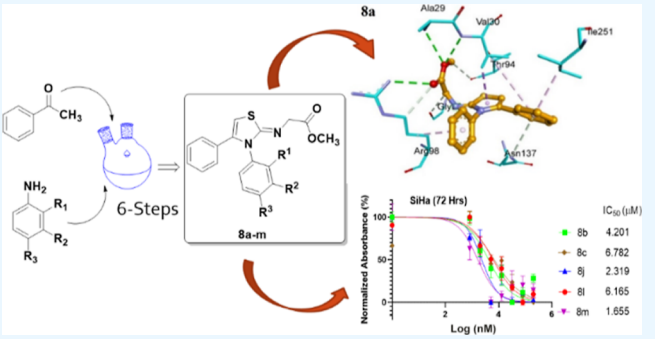

1. INTRODUCTION

Cancer cells present largely different bioenergetics than normal cells and are dependent on an enhanced rate of tumor glycolysis.[1] Cancer cell metabolism, specifically tumor glycolysis, has emerged as a unique cancer phenotype due to higher consumption of glucose resulting in higher lactate production in cancer cells than in normal cells even under normoxic conditions. Consequently, tumor glycolysis creates acidosis in the extracellular matrix, which facilitates tumor initiation, progression, invasion, and metastasis.[2] Enhanced rate of tumor glycolysis in cancer cells ensures their high energy and metabolite demand, resulting in excess lactate and H^+ ion production, which is then transported outside the cell by MCT enzymes and establishes the lactate flux.[3−5] Therefore, cancer cells are characterized by an enhanced rate of tumor glycolysis controlled by the overexpression of several enzymes, cofactors, and transporters. A very close association between cancer cell metabolism and cancer stemness was also established.[6] Cancer cells represent common characteristic features such as an enhanced rate of aerobic glycolysis, a higher rate of glucose consumption and lactate production, and an increased rate of extracellular acidosis, which can be exploited for drug development.[7−10] Therefore, tumor glycolysis is considered a novel target in search of better cancer treatment options. Moreover, in normal cells, the last step of glycolysis produces pyruvate, which is considered an energy hub from where pyruvate goes along with three distinct pathways: (i) formation of lactate; (ii) conversion to acetyl-CoA, and (iii) conversion to alanine. Conversely, in cancer cells, most of the pyruvate is reduced to lactate coupled with the oxidation of NADH to NAD^+ catalyzed by the Lactate Dehydrogenase (LDH) enzyme.[7−10] The LDH enzyme is a tetrameric protein composed of two different subunits *ldha* and *ldhb*, which are encoded by two separate genes *ldha* and *ldhb*, respectively. In humans, LDH exists in four isoforms formed by various possible combinations of these two subunits. Among these, the

Received: November 26, 2022
Accepted: April 24, 2023
Published: May 10, 2023

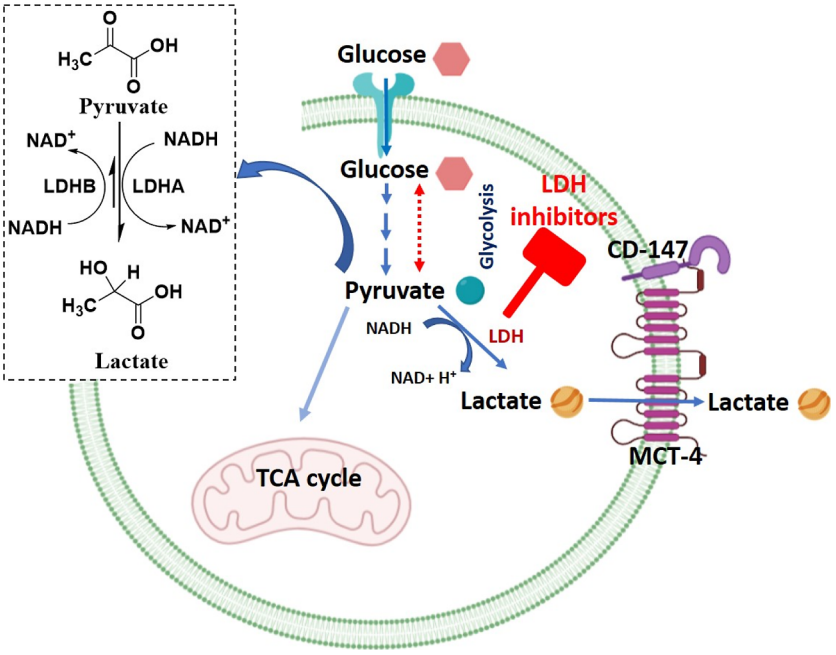

Figure 1. LDH inhibition through LDH inhibitors kill cancer cells.

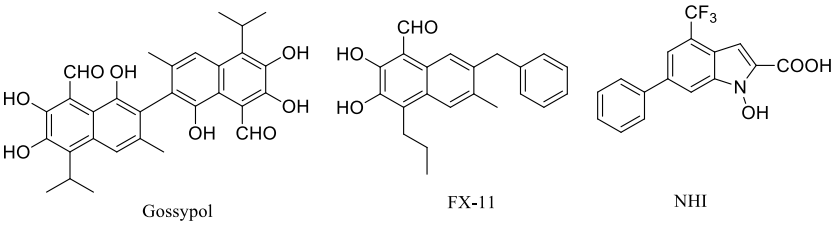

Figure 2. Chemical structure of potential *h*LDH5 inhibitors.

LDHA and LDHB are homoisomers of *ldha* and *ldhb* subunits, respectively (Figure 1).[7] The human LDHA (*h*LDHA) enzyme is overexpressed in almost all metabolic cancer and exists at the end of tumor glycolysis[7,11] at the bifurcation point of pyruvate, which makes it a viable target from where the selective inhibition of *h*LDHA can selectively kill the cancer cells *via* blocking energy and metabolites supply (Figure 1).[11]

Potential small molecules acting as *h*LDHA inhibitors can kill cancer cells by serving as starving agents.[5] Several small molecules including natural and synthetic compounds with molecular diversity exhibiting significant *h*LDHA inhibitory activity have been discovered; however, very few have entered clinical trials.[7−11] For example, the nonselective natural product gossypol entered into clinical trial but failed due to side effects that may arise due to the presence of aldehyde functional groups (Figure 2). Later, the FX-11 analogue of half gossypol was discovered, which showed potential *h*LDHA inhibitory activity (Figure 2). A new class of *N*-hydroxy indole-based *h*LDHA inhibitor (NHI) was developed, which showed significant selectivity (Figure 2).[12−16] Although several molecules have been discovered,[17−19] still there is a large chemical gap available to discover new *h*LDHA inhibitors as potential anticancer agents.

Herein, we have designed a distinguished class of small molecules based on a central scaffold thiazole using an *in silico* approach[20] to disrupt the tumor glycolysis by inhibiting the *h*LDHA enzyme. Small molecules including thiazole heterocycles displayed a wide range of biological activities and play an important role in medicinal chemistry and drug discovery.[21−25] It is an essential part of several natural products such as vitamin B1- Thiamine and several synthetic anticancer drugs; thus, thiazole core-based molecules and hybrid structures would be potential anticancer compounds.[26] Lipophilic properties of di-substituted thiazole at two positions make these compounds efficient for transport through a biological membrane. In this paper, we studied the molecular interaction of this different class of small molecules with the *h*LDHA by molecular docking, synthesized high-scored molecules, and screened them for *h*LDHA activity evaluation. The most potent molecules were further screened for anticancer activity evaluation in cancer cell lines, and their pharmacokinetic profile was evaluated.

2. RESULTS AND DISCUSSION

2.1. Pharmacophore Requirement of the Designed Molecules. The binary and ternary X-ray crystal of *h*LDH5 or LDHA subunit with the cofactor (NADH) and substrate (pyruvate) shows that the binding pocket is small, and the active site is situated in a deep position; thus, accessibility of the compound to the binding cavity is narrow.[12] The binding cavity holds both the substrate and cofactor and is rich in arginine amino acids, which are cationic residues. Thus, the overall binding cavity is polar and cationic; therefore, most of the inhibitors discovered so far have a carboxylate functional group. In some inhibitors, the carboxylate group is in close proximity with hydroxyl and carbonyl groups, which act as the

https://doi.org/10.1021/acsomega.2c07569
ACS Omega 2023, 8, 17552−17562

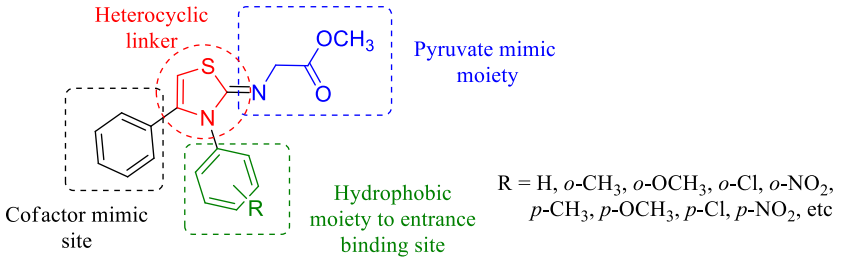

Figure 3. Basic pharmacophore model for target molecules.

surrogates of the substrate of *h*LDHA. Considering these pharmacophore requirements, we have designed a series of molecules based on a thiazole central scaffold having a carboxylate group which is part of the aliphatic ring and two aromatic rings that are directly bonded with the thiazole scaffold (Figure 3). This type of series has never been explored before, and such type of unusual class of molecules based on a thiazole scaffold is an important class of molecules with pharmaceutical values.

2.2. Molecular Docking Study. Molecular docking studies of all designed compounds (Figure 4, Tables 1 and S1) were performed using software ChemDraw (https://chemdrawdirect.perkinelmer), AutoDock (https://autodock.scripps.edu/), Chimera (https://www.cgl.ucsf.edu/chimera), and PyMOL (https://pymol.org/2/). The geometry of the molecules was optimized using Avogadro software (http://avogadro.openmolecules.net.) The structure of all the molecules was made by using ChemDraw and then transformed into a 3D structure suitable for docking using Avogadro (https://two.avogadro.cc/) and OpenBabel software (https://open-babel.soft). To examine the best possible binding modes of a compound in the binding cavity of *h*LDHA (PDB ID: 1I10), AutoDock was used, and protein-docked compound images were prepared using Chimera or PyMOL software. All the docking poses were ranked to calculate the ΔG bind values to attain acceptable levels of *h*LDHA inhibition within this chemical class. To obtain the structure−activity relationship (SAR) R^1, R^2, and R^3 were selected as both the electron-withdrawing and electron-donating groups at the ortho, meta, and para positions, respectively (Figure 4, Tables 1 and S1).

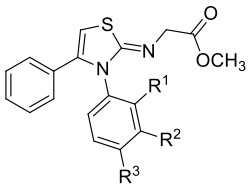

Figure 4. Structure of target molecules.

Docking results of the designed molecules with *h*LDHA were found in the range of −9.8−−6.2 kcal/mol and are summarized in Table 1. In compound **8a**, R^1═R^2═R^3═H showed strong binding affinity, exhibiting a binding energy of −8.8 kcal/mol. When H of the ortho position was replaced by the OCH_3 leading to **8b** (R^1═OCH_3) showed a minor reduction in binding affinity (−8.1 kcal/mol) might be due to −I effect as well as due to the electron pair of O atom of $-OCH_3$, served resonance effect (+R) and can lose an electron. Further, if a stronger electron-withdrawing group, *i.e.*, NO_2, was inserted at the ortho position (**8c,** R^1═NO_2), the binding energy significantly increases to −9.8 kcal/mol. Besides, the insertion of an electron-donating group CH_3 at the ortho position (**8d,** R^1═CH_3) slightly decreases the binding energy to −8.5 kcal/mol. In the case of **8e**, the electron-withdrawing group "−Cl" (also served resonance effect, +R) at ortho position showed reduced binding affinity, as Cl exhibits a strong −I effect, and +R. Moreover, the substitution of the electron-withdrawing group OCH_3, NO_2, and Cl and the electron-donating group CH_3 at the meta position (R^2) showed lower binding affinity (Table 1) than substitution at the ortho position. Further, substitution on the para position (R^3) by an electron-withdrawing group as well as an electron-donating group showed better results than substitution on the meta position; however, electron-withdrawing groups at the ortho position were found to be the preferred position for enhanced binding affinity.

Molecular docking analysis of the designed molecules with the *h*LDHA (PDB ID: 1I10) enzyme revealed that all the molecules showed a common binding mode and presented similar types of binding interactions in the binding cavity of *h*LDHA (Figure 5). The analysis revealed that amino acids Ala 29, Val 30, Arg 98, Gln 99, Gly 96, and Thr 94 play an important role to possess strong interaction with the compounds (Figure 5). More specifically, the complex structure of *h*LDHA with **8c** indicates that NO_2 at the ortho position showed interaction with Gln 99 through hydrogen

Table 1. Defined R^1, R^2, and R^3, Binding Energy (kcal/mol) of Compounds 8a−8m

S. no.	compounds no.	R^1, R^2, R^3	binding energy (kcal/mol)	S. no.	compounds no.	R^1, R^2, R^3	binding energy (kcal/mol)
1.	8a	R^1═R^2═R^3═H	−8.8	8.	**8h**	R^1═R^2═CH_3, R^3═H	−7.0
2.	8b	R^1═OCH_3, R^2═R^3═H	−8.1	9.	**8i**	R^1═H, R^2═Cl, R^3═H	−7.2
3.	8c	R^1═NO_2, R^2═R^3═H	−9.8	10.	**8j**	R^1═R^2═H, R^3═OCH_3	−7.1
4.	8d	R^1═CH_3, R^2═R^3═H	−8.5	11.	**8k**	R^1═R^2═H, R^3═NO_2	−6.2
5.	8e	R^1═Cl; R^2═R^3═H	−7.2	12.	**8l**	R^1═R^2═H, R^3═CH_3	−7.6
6.	8f	R^1═H; R^2═OCH_3, R^3═H	−6.3	13	**8m**	R^1═R^2═H; R^3═Cl	−7.6
7.	8g	R^1═H; R^2═NO_2, R^3═H	−6.4				

https://doi.org/10.1021/acsomega.2c07569
ACS Omega 2023, 8, 17552−17562

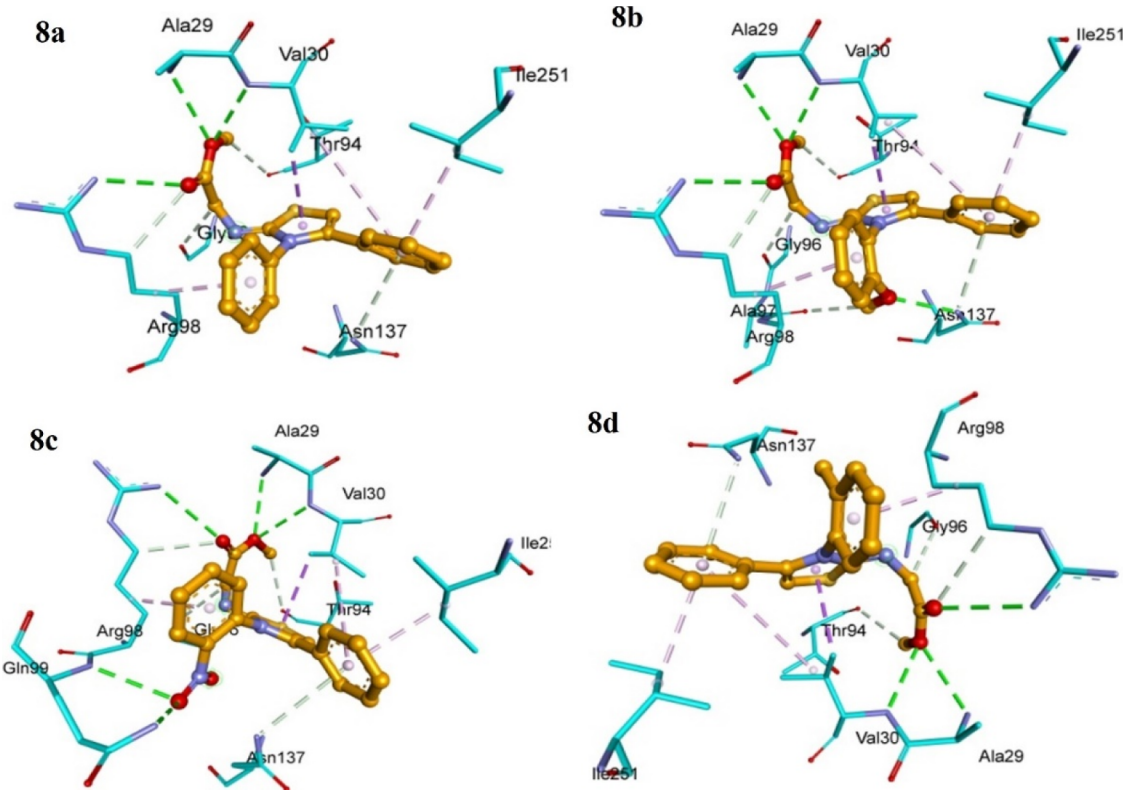

Figure 5. Compounds **8a**, **8b**, **8c**, and **8d** complexed with *h*LDHA (PDB ID: 1I10).

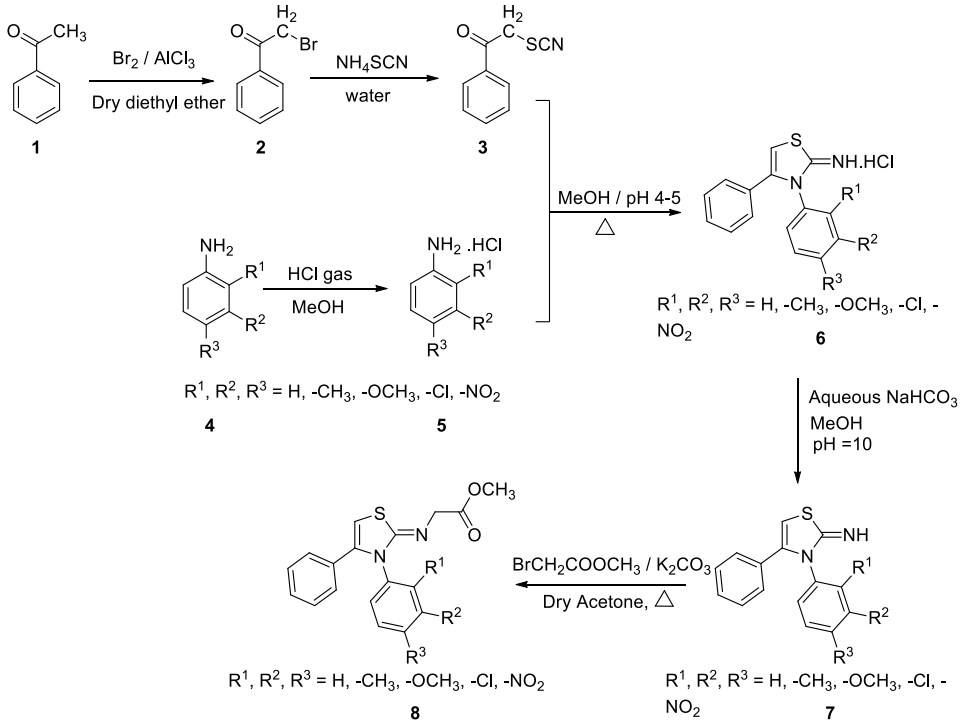

Figure 6. Synthetic scheme for the synthesis of final compounds **8a−d**, **8j**, **8l**, and **8m.**

bonding. The OCH_3 of ester exhibited interaction with Ala 29 and Val 30, whereas oxygen of the carbonyl of the ester exhibited interaction with Arg 98 (Figure 5). Based on docking results, **8a−d** and **8l** were selected for synthesis and biological studies.

2.3. Chemistry. Selected high-scored compounds **8a−d**, **8j**, **8l**, and **8m** were synthesized from *N*-alkylation of the final intermediates **7a−d**, **7j**, **7l**, and **7m** with the reaction of methyl 2-bromoacetate in the basic medium at 80 °C in dry acetone as a solvent in the presence of potassium carbonate (Figure 6). The thiazole central scaffold-based starting materials **7a−d**, **7j**,

https://doi.org/10.1021/acsomega.2c07569
ACS Omega 2023, 8, 17552−17562

7l, and **7m** for final compounds were synthesized by following a reported synthetic protocol with slight modification to improve the yield using acetophenone.[27,28]

All the starting materials (**7a−d**, **7j**, **7l**, and **7m**) were characterized by ^{1}HNMR and mass spectrometry for further reaction. Catalytic bromination of acetophenone (**1**) using bromine in the presence of Lewis catalyst $AlCl_3$ in dry ether resulted in 2-bromo-1-phenylethanone (**2**), which on treatment with an aqueous solution of ammonium thiocyanate yielded the phenacyl thiocyanate (**3**, 1-phenyl-2-thiocyanatoethanone). The condensation of phenacyl thiocyanate (**3**) with various respective amine hydrochlorides (**5a−d**, **5j**, **5l**, and **5m**) in dry methanol maintaining pH 4−5 under nitrogen resulted in hydrochloride salts of compounds **6a−d**, **6j**, **6l**, and **6m**. So obtained hydrochloride salts **6a−d**, **6j**, **6l**, and **6m** on treating with aqueous NaOH at pH ∼ 10 led to compounds **7a−d**, **7j**, **7l**, and **7m**, which were used as starting materials for the synthesis of target compounds. All the synthesized compounds **8a−d, 8j, 8l,** and **8m** were purified by column chromatography and the structure of compounds **8a−d, 8j, 8l,** and **8m** were confirmed by ^{1}H and ^{13}C NMR and mass spectrometry.

2.4. Biological Activities. *2.4.1. hLDHA Inhibitory Activities.* The pure and well-characterized compounds **8a−h** were screened for *h*LDHA inhibitory activities using the reported protocol.[16] For *h*LDHA inhibitory activities, compounds were dissolved in DMSO, and then dilutions were made using sterile water. In all the biological screenings, the concentration of DMSO was kept below 1%. To determine the inhibitory potencies, compounds were screened on *h*LDHA in competition with substrate pyruvate by measuring the change in the intensity of NADH *via* oxidation at pH 7.2. The decrease in NADH fluorescence or absorbance was followed by a spectrofluorometer (BioTek USA) at 340 nm excitation and 460 nm emission wavelengths. The total volume used in each well was 200 μL, which constitutes 152 μL of NADH, sodium pyruvate in PBS buffer, 8 μL compound, and 40 μL of the *h*LDHA enzyme. The percentage inhibition is calculated assuming 100% inhibition with the reference summarized in Table 2. The *h*LDHA enzyme inhibitory screening of the selected compounds showed that compounds **8a** and **8b** showed a moderate inhibitory effect against the *h*LDHA enzyme in competition with the substrate pyruvate. Compounds **8b**, **8c**, **8d**, **8j**, and **8l** showed good enzyme inhibitory activities *i.e.*, 48, 53, 43, 49, and 52% in competition with pyruvate. Among all, compounds **8c** and **8l** endowed approximate same enzyme inhibitory activities, whereas other compounds showed moderate inhibitory effect against the *h*LDHA enzyme.

Table 2. Percentage Inhibitory *h*LDHA Activity of 100 μM Repeated in Triplicate and cLogp Values

compd. no.	% inhibitory *h*LDHA activity (μM)	cLogp	compd. no.	% inhibitory *h*LDHA activity (μM)	cLogp
8a	33	2.489	**8j**	49	3.555
8b	48	3.555	**8l**	52	4.135
8c	53	3.379	**8m**	41	4.349
8d	43	4.135			

The percentage *h*LDHA inhibitory activity of compounds **8a−d, 8j, 8l,** and **8m** was measured at 100 μM concentration using the following equation

$$\% \text{ inhibition} = 100 \times [1 - (X - \min)/(\max - \min)]$$

$$\max = \text{absorbance with no inhibition}$$

$$\min = \text{absorbance with 100\% inhibition}$$

$$X = \text{absorbance at the given concentration of synthesized inhibitor}$$

All compounds **8a−d, 8j, 8l,** and **8m** showed inhibitory *h*LDHA activities having an acceptable cLogp value and were considered for further biological activities' evaluation. The cLogp values of all compounds were calculated by software ChemDraw version 12.0 for measurement of hydrophilicity and are reported in Table 2.

2.4.2. In Vitro Cytotoxicity of Target Compounds. *In vitro* cytotoxicity against various human cancer cell lines was determined using a reported protocol.[29] The selected compounds (**8a−d**, **8j**, **8l**, and **8m**) were screened for anticancer activity in six cancer cell lines including human Pancreatic Ductal Adenocarcinoma (02.03, 04.03 and 03.27), liver cancer cells (HepG2), cervical cancer cell lines (HeLa and SiHa), and human embryonic kidney cells (HEK-293). Cancer cells were grown in Dulbecco's modified Eagle's medium (DMEM) containing 10% fetal serum albumin and 1% antibiotic/antimycotic solution. All the cultures were maintained at 37 °C in an incubator containing 5% CO_2. Both normal and cancer cells were seeded in 96-well plates (5.0×10^5cells per well). The cells were exposed to serially diluted concentrations of compounds with a starting concentration of 100 μM. Non-treated control cells were also maintained in the same conditions to compare the growth inhibition. The content in all respective wells including tests and control was decanted after 72 h of treatment and 20 μL of reconstituted MTT (Sigma) was added. After 2 h of dark incubation in a 5% CO_2 humidified incubator, the supernatant was removed and 100 μL of MTT solubilization solution was added and kept in a shaking incubator at 37 °C to solubilize formazan crystals. The absorbance was recorded at 570 nm using a microplate reader. The experiments were performed in triplicate, and the cell viability was calculated from the curves of the mean OD values and plotted against the drug concentration. The IC_{50} value was analyzed using GraphPad Prism 8 reported in Table 3 and Figure 7.

2.4.2.1. In Vitro Cytotoxicity in Human PDAC (02.03, 03.27, and 04.03) Cell Lines. These compounds showed moderate activity against all three (02.03, 03.27, and 04.03) cancer cell lines. Compound **8a**, where R^1, R^2 and R^3 are H, showed moderate activity in the high micromolar range against 02.03 and 03.27 cancer cell lines, whereas it was found inactive against 04.03 cell lines (Table 3, Figures 7 and S1). When hydrogen at the ortho position (R^1=H) was replaced by electron-withdrawing group OCH_3, the resulting compound **8b** showed improved inhibitory activity against 02.03, 03.27, and 04.03 cancer cell lines exhibiting IC_{50} values of 40.12, 13.48, and 52.23 μM, respectively (Table 3, Figures 7, S2 and S3). Insertion of a more electron-withdrawing group $-NO_2$ at the ortho position leads to compound **8c** that further enhanced the inhibitory effect on both 03.27 and 04.03 cancer lines; however, for 02.03 cancer cell lines, inhibitory activity decreases (Table 3, Figure 7). When the electron-donating group ($-CH_3$) was inserted at the ortho position in place of the withdrawing group ($-OCH_3$), the resulting compound **8d** showed a reduction in inhibitory activity against all the three

https://doi.org/10.1021/acsomega.2c07569
ACS Omega 2023, 8, 17552−17562

Table 3. *In Vitro* Cytotoxicity (IC_{50}) of Compounds 8a−d, 8j, 8l, and 8m against Pancreatic, Liver, and Cervical Cancer Cell Lines[a]

		cancer cells					
		pancreatic IC_{50} (μM)			liver IC_{50} (μM)	cCervical IC_{50} (μM)	
S. no	tested comp.	02.03	03.27	04.03	HepG2	HeLa	SiHa
1.	**8a**	81.50	72.23	>100	75.50	NT	NT
2.	**8b**	40.12	**13.48**	52.23	22.66	**2.97**	**4.20**
3.	**8c**	>100	25.50	22.10	15.38	**6.02**	**6.78**
4.	**8d**	>100	>100	>100	79.20	NT	NT
5.	**8j**	72.20	**11.51**	75.20	**7.90**	**6.75**	**2.32**
6.	**8l**	61.23	**10.84**	50.32	83.68	**8.65**	**6.16**
7.	**8m**	23.22	22.08	52.10	**5.15**	16.96	**1.65**
8.	**doxorubicin**				1.1[30]	0.14[31]	8.3[32]
9.	**gemcitabine**	0.38	0.42	0.19			

[a]Data were obtained as mean SD from 3 independent repeats (n = 3).

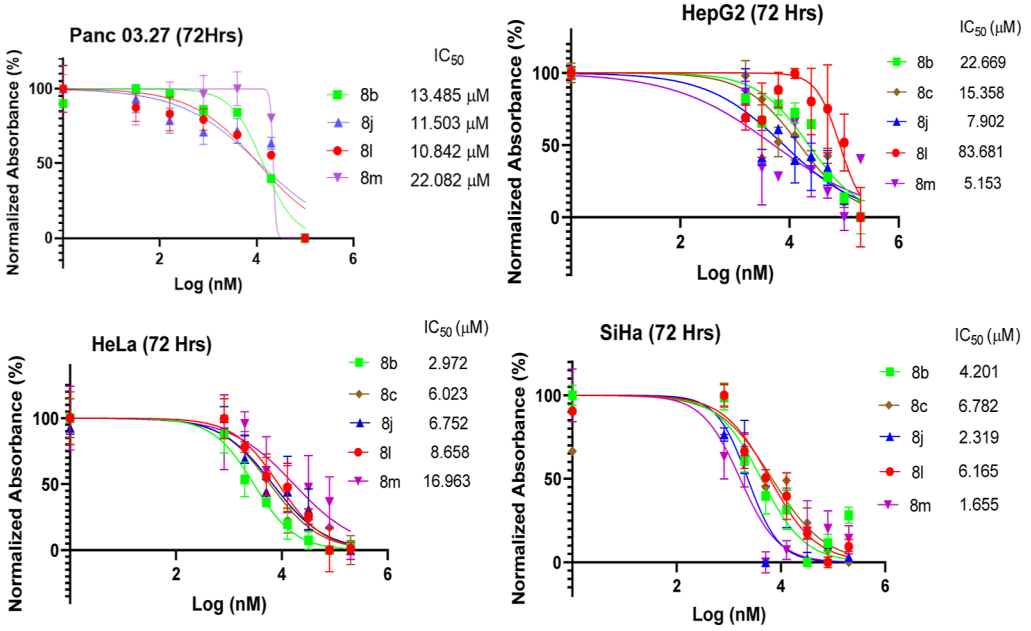

Figure 7. IC_{50} values of most active compounds on Panc 03.27, HepG2, HeLa, and SiHa cancer cell lines.

PDAC cancer cell lines. Upon insertion of the electron-withdrawing group OCH_3 at the para position, the resulting compound **8j** exhibited a significant inhibitory effect on PDAC 03.27 having an IC_{50} value of 11.50 μM. However, it showed moderate activity against 02.03 and 04.03 cancer cell lines in the high micromolar range. Compound **8l** where the electron-donating group ($-CH_3$) was placed at the para position exhibited an IC_{50} value of 10.84 μM against the PDAC 03.27 cancer cell lines. In addition, if the -Cl was placed at the para position, the resulting compound **8m** showed moderate activity in the low micromolar range (Table 3, Figure 7). These data suggest that the electron-withdrawing groups are a better choice than the electron-donating groups at the ortho position for the development of more potent compounds in this series. Moreover, the substitution at the ortho position is preferable over the para position.

2.4.2.2. In Vitro Cytotoxicity in the Liver (HepG2) Cancer Cell Line. Compound **8a** (where R^1, R^2, and R^3 are H) showed moderate activity against HepG2, exhibiting IC_{50} values of 75.50 μM (Table 3, Figures 7 and S4). Compound **8b**, where hydrogen at the ortho position (R^1=H) was replaced by the electron-withdrawing group (R^1=OCH_3), showed a marked increment in inhibitory activity, showing IC_{50} values of 22.66 μM. Compound **8c** showed a significant increment in inhibitory activity, having IC_{50} value of 15.38 μM in liver cancer cells (HepG2). In the case of compound **8l**, R^3=CH_3 showed a marked reduction in anti-cancer activity, with an IC_{50} value of 83.68 μM. In compound **8m**, Cl is placed at the para position and is endowed an IC_{50} value of 5.15 μM HepG2 (Table 3, Figure 7). Electron-withdrawing groups are a better choice than the electron-donating groups at the ortho position for the development of more potent compounds.

2.4.2.3. In Vitro Cytotoxicity in the Cervical (HeLa) Cancer Cell Line. Results of *in vitro* cytotoxicity against the cervical (HeLa) cancer cell line revealed that the substitution on the ortho position by the OCH_3 moiety resulted in compound **8b** (R^1=$-OCH_3$), which showed a marked increment in inhibitory activity, exhibiting IC_{50} values of 2.97 μM against the HeLa cell line (Table 3, Figures 7 and S5). Further substitution at the same position by the $-NO_2$ group leads to compound **8c** showing very good inhibitory activity, with an IC_{50} value of 6.02 μM in HeLa; however, it showed less activity

https://doi.org/10.1021/acsomega.2c07569
ACS Omega 2023, 8, 17552−17562

Table 4. Molecular Weight, iLOGP, Consensus Log Po/w, Number of Hydrogen Bond Acceptors and Donors

S. no.	compound name	molecular weight	log Po/w (iLOGP)	consensus log Po/w	GI absorption	drug likeness (Lipinski)	log S
1.	**8a**	324.40	3.37	3.61	high	yes	−4.49
2.	**8b**	354.42	3.49	3.57	high	yes	−4.54
3.	**8c**	369.39	3.15	2.89	high	yes	−4.54
6.	**8j**	354.42	3.63	3.60	high	yes	−4.54
7.	**8l**	338.42	3.63	3.95	high	yes	−4.76
8.	**8m**	358.84	3.66	4.15	high	yes	−5.08

than **8b**. Compound **8j** of this series showed almost similar activity to **8c**, exhibiting an IC_{50} value of 6.75 μM (Table 3, Figure 7). Moreover, for compound **8l** (R^3=CH_3), substitution by CH_3 at the para position showed a small reduction in anticancer activity, possessing an IC_{50} value of 8.65 μM, which was found lower than those of **8b**, **8c**, and **8j**. However, it exhibited better activity than compound **8m** where Cl is placed at the para position, exhibiting an IC_{50} value of 16.96 μM in the HeLa cancer cell lines (Table 3, Figure 7). Moreover, substitution on the ortho preferred is preferred position over the para position. These results were found in agreement with the *h*LDHA inhibitory activities and *in silico* binding affinities.

2.4.2.4. In Vitro Cytotoxicity in the Cervical (SiHa) Cancer Cell Line. *In vitro* cytotoxicity results against the cervical (SiHa) cancer cell line revealed that compound **8b** (R^1=OCH_3, R^2=R^3=H) showed good inhibitory activity in SiHa, with IC_{50} values of 4.20 μM (Table 3, Figures 7 and S6). Further substitution at the same position by the NO_2 group leads to compound **8c**, which showed slightly lower inhibitory activity, having an IC_{50} value of 6.78 μM. Compound **8j** (R^3=OCH_3), where methoxy group is present at the para position, showed an increment in inhibitory activity, exhibiting an IC_{50} value of 2.32 μM (Table 3, Figure 7). Moreover, for compound **8l** (R^3=CH_3), substitution by CH_3 at the para position showed similar activity to **8c** with small reduction with respect to **8j** in inhibitory activity possessing an IC_{50} value of 6.16 μM. Compound **8m,** where −Cl is placed at the para position, exhibited an IC_{50} value of 1.65 μM, which was found to be the most active compound of this series (Table 3, Figure 7).

2.4.2.5. In Vitro Cytotoxicity in Human Embryonic Kidney Cells (HEK293). To test the selectivity of the most active compounds **8j** and **8m**, we have carried out the MTT assay in human embryonic kidney cells (HEK293). *In vitro* cytotoxicity results indicate that these molecules are cytotoxic to cancer cells and do not induce toxicity to healthy cells (Figure S7).

In vitro cytotoxicity data revealed that substitution at the ortho position is preferred over the para position. Moreover, electron-withdrawing groups exhibit better *in vitro* cytotoxicity than electron-donating moieties. The *in vitro* activities of the compounds were found in agreement with the *h*LDHA inhibitory activities and *in silico* screening. The cLogP values of these compounds were found in the range of 2.489−4.349 and considered acceptable. The *h*LDHA inhibitory activities and IC_{50} suggested that clogP in the range of 3.379 to 4.135 favors the inhibitory activities.

2.5. *In Silico* Predictive ADMET Study. The absorption, distribution, metabolism, excretion, and toxicity (ADMET) are evaluated for **8a**, **8b**, **8c**, **8j**, **8l**, and **8m** using SwissADME (http://www.swissadme.ch/) (Figures S8−S13). Several parameters were considered, *viz*, number of hydrogen bond donors and acceptors, blood−brain barrier level, absorption level, 2D polar surface area (ADMET 2D PSA), Cytochrome P450 2D6 (CYP2D6), hepatotoxicity probability, aqueous solubility level, and plasma protein binding logarithmic level and calculated by SwissADME. Biorelevant small molecules under consideration are ideal drug-like candidates with good bioavailability and follow the Lipinski rule, which implies the following features, *i.e.*, mw ≤ 500, log P ≤ 5, number of hydrogen bond acceptors ≤ 10 (*i.e.*, N or O atoms), and hydrogen bond donors ≤ 5 (Lipinski *et al.*[33]). These rules of five were used to investigate the drug-likeness of all **8a**−**h** thiazole-based compounds, and data are summarized in Table 4

Data summarized in Table 4 suggest that compounds have mw ≤ 500, log P, log P ≤ 5. The number of hydrogen bond acceptors in all the compounds lies in the range of 3 to 5, which follows Lipinski's rule of five where hydrogen bond acceptors should be ≤ 10 including N or O atoms and hydrogen bond donors ≤ 5. All compounds showed clogP (Table 2) values in the range of 2.62 to 4.15. *In silico* ADME profiling shows that all the investigated compounds follow Lipinski's rule of drug-likeness.

2.6. Structure−Activity Relationship. In the thiazole central scaffold-based compounds (**8a-d**, **8j**, **8l**, and **8m**), the substitution at the ortho, meta, and para positions on the N substituted aromatic ring showed that these compounds showed better activity against cervical SiHa and HeLa cancer cells than the liver (HepG) cancer cell and are least active on pancreatic cancer cells. The substitution by an electron-withdrawing group at ortho position (R^1) showed better activity for HepG, SiHa, and HeLa cancer cell lines. Compounds **8b**, **8j,** and **8l** showed good activity on 03.27 pancreatic cancer cell lines and the rest of the molecules showed moderate activity against all three 02.03, 03.27, and 04.03 pancreatic cancer cell lines. All compounds showed better anticancer activity against HepG-2 cell lines than pancreatic cancer cell lines. Compounds **8b**, **8c**, **8j**, **8l,** and **8m** exhibited good anticancer activity against cervical SiHa and HeLa cancer cell lines.

2.7. Conclusions. A new series of thiazole central scaffold-based small molecules **8a**−**d**, **8j**, **8l**, and **8m** were synthesized and screened for *h*LDHA inhibitory activities. *In silico* binding affinity of these compounds was calculated against the *h*LDHA enzyme. The *h*LDHA inhibitory activities showed that compounds **8c**, **8d**, **8e**, **8j,** and **8m** have adequate inhibitory activities, which are consistent with an *in silico* study. Molecular docking studies depicted that the Ala 29, Val 30, Arg 98, Gln 99, Gly 96, and Thr 94 amino acids of *h*LDHA strongly interacted with compounds through hydrogen bonding and electrostatic and hydrophobic interaction, which might play important roles in inhibitory activities. *In vitro* anticancer activity evaluation depicted that compounds **8j** and **8m** were most active against HepG2 cancer cells possessing IC_{50} values of 7.9 and 5.15 μM. Compounds **8b**, **8j**, and **8m** showed IC_{50}

https://doi.org/10.1021/acsomega.2c07569
ACS Omega 2023, 8, 17552−17562

values of 4.2, 2.32, and 1.66 μM, respectively, against the SiHa cancer cell line, whereas **8b** also showed inhibitory activity against HeLa cancer cell lines having an IC_{50} value of 2.97 μM. However, in pancreatic cancer cell lines, all the compounds showed a moderate effect. Compounds **8j** and **8m** did not exhibit toxicity on healthy cells (HEK293). Overall, the compounds of this series showed very good anticancer activities and selectivity in HeLa and SiHa cervical cancer cell lines. Inspired by these results, similar analogues of most active molecules may be explored for cancer therapeutics.

3. EXPERIMENTAL SECTION

3.1. General. All the chemicals and reagents were purchased from Sigma-Aldrich, SRL, and Sd fine and were used without further purification. The *h*LDHA enzyme was purchased from Sigma-Aldrich. Pancreatic cancer cells (02.03, 04.03, 03.27) and liver cancer cells (HepG2) were purchased from ATCC and NCCS, respectively. Gemcitabine was procured from Selleckchem. Stock solution of 1 mM was prepared in DMSO and used for *in vitro* cytotoxicity analysis in pancreatic cancer cells. Thin-layer chromatography (TLC) was performed on silica gel 60 F254 Merck KGaA Germany, and spots were visualized by iodine vapor or by irradiation with ultraviolet light (254 nm). Silica gel of 100−200 mesh was obtained for column chromatography. Melting points (mp) of all **7a−d, 7j, 7l,** and **7m** and **8a−d, 8j, 8l,** and **8m** were calculated on a JSGW apparatus and are uncorrected. Solvent DMSO was used for NMR purchased from Sigma. NMR spectra were recorded on a Bruker WH-400 spectrometer or JEOL 400 MHz instrument at a *ca.* 5−15% (w/v) solution in DMSO-d_6. Mass spectra were recorded on a Q EXACTIVE PLUS, Thermo Scientific spectrometer. Elemental analysis was carried out on a Vario ELIII elementor. HPLC analysis was performed on Shimadzu LC-2030C 3D plus using column XTIMATE C18 and flow rate 1.0 mL/min.

*3.1.1. General Procedure for the Synthesis of Phenacyl Thiocyanate (**3**).* Phenacyl thiocyanate was synthesized in 96% yield by the reaction of phenacyl bromide with ammonium thiocyanate in methanol by using a literature protocol with slight modifications.[27,28] Herein, saturated ammonium thiocyanate solution was used to generate thiocyanate nucleophiles. Nucleophilic substitution reaction of phenacyl bromide with thiocyanate nucleophile in a methanol/water solution resulted in the desired phenacyl thiocyanate. However, in the literature protocol, $KSCN/SiO_2-RNH_3OAc/Al_2O_3$, NaSCN, and KSCN have been used to generate nucleophiles.

*3.1.2. General Procedure for the Synthesis of Various 3,4-Diphenylthiazol-2(3H)-imine (**7a−h**).* These starting materials were prepared by following a reported synthetic procedure with a slight modification.[28] Phenacyl thiocyanate **3** (1 mmol) was placed in a round bottom flask in dry methanol under nitrogen. Once the clear solution formed, aniline hydrochlorides (**5a−d, 5j, 5l,** and **5m**) (1 mmol) were added to the reaction vessel, and then the reaction mixture was allowed to heat at 70 °C with continuous stirring for 7 h. Reaction progress was monitored by TLC. Once the reaction was completed, the solvent was removed under reduced pressure. The solid residue so obtained was dissolved in methanol/water at a (1:1) ratio and the reaction content was basified using an aqueous solution of NaOH up to pH 10−11 to precipitate out the desired compound. The precipitate so obtained was filtered and recrystallized in an appropriate solvent to give pure products **7a−d, 7j, 7l,** and **7m**. Melting points and NMR spectral data of reported compounds **7a−d, 7j, 7l,** and **7m** were inconsistent with the synthesized compounds.

*3.1.2.1. 3,4-Diphenylthiazol-2(3H)-imine (**7a**).* The solvent of crystallization was EtOH; yield 90%; solid; mp: 85.3 °C; ^{1}H NMR (400 MHz; DMSO-d_6) δ 6.48 (s, 1H, >C═CH), 7.14−7.16 (m, 2H, Ar), 7.33−7.34 (m, 3H, Ar), 7.42−7.44 (m, 2H, Ar), 8.18−8.19 (m, 2H, Ar), 8.45 (s, 1H, NH exch).

*3.1.2.2. 3-(2-Methoxyphenyl)-4-phenylthiazol-2(3H)-imine (**7b**).* The solvent of crystallization was EtOH; yield 83%; solid; mp: 91.4 °C; ^{1}H NMR (400 MHz; DMSO-d_6) δ 3.52 (s, 3H, OCH_3), 6.13 (s, 1H, >C═CH), 6.89−6.95 (m, 2H, Ar), 7.04−7.06 (m, 2H, Ar), 7.14−7.18 (m, 3H, Ar), 7.23−7.28 (m, 2H, Ar), 7.65 (s, 1H, NH exch).

*3.1.2.3. 3-(2-Nitrophenyl)-4-phenylthiazol-2(3H)-imine (**7c**).* The solvent of crystallization was EtOH; yield 86%; solid; mp: 125.3 °C; ^{1}H NMR (400 MHz; DMSO-d_6) δ 6.24 (s, 1H, >C═CH), 7.10−7.12 (m, 3H, Ar), 7.20−7.22 (m, 3H, Ar), 7.46−7.56 (m, 2H, Ar), 7.97−7.99 (m, 1H, Ar), 8.21 (s, 1H, NH exch).

*3.1.2.4. 4-Phenyl-3-(o-tolyl)thiazol-2(3H)-imine (**7d**).* The solvent of crystallization was EtOH; yield 89%; solid; mp: 108.1 °C; ^{1}H NMR (400 MHz; DMSO-d_6) δ 2.23 (s, 3H, CH_3), 6.18 (s, 1H, >C═CH), 6.97−7.99 (m, 2H, Ar), 7.09−7.12 (m, 4H, Ar), 7.15−7.18 (m, 3H, Ar), 7.65 (s, 1H, NH exch).

*3.1.2.5. 3-(4-Methoxyphenyl)-4-phenylthiazol-2(3H)-imine (**7j**).* The solvent of crystallization was EtOH; yield 88%; solid; mp: 98.4 °C; ^{1}H NMR (400 MHz; DMSO-d_6) δ 3.67 (s, 3H, OCH_3), 6.19 (s, 1H, >C═CH), 6.82−6.84 (m, 2H, Ar), 7.00−7.07 (m, 2H, Ar), 7.08−7.09 (m, 2H, Ar), 7.16−7.19 (m, 3H, Ar), 7.68 (s, 1H, NH exch).

*3.1.2.6. 4-Phenyl-3-(p-tolyl)thiazol-2(3H)-imine (**7l**).* The solvent of crystallization was EtOH; yield 89%; solid; mp: 108.4 °C; ^{1}H NMR (400 MHz; DMSO-d_6) δ 2.21 (s, 3H, CH_3), 6.19 (s, 1H, >C═CH), 6.96−7.98 (m, 2H, Ar), 7.06−7.08 (m, 4H, Ar), 7.16−7.18 (m, 3H, Ar), 7.62 (s, 1H, NH exch).

*3.1.2.7. 3-(4-Chlorophenyl)-4-phenylthiazol-2(3H)-imine (**7m**).* The solvent of crystallization was EtOH; yield 78%; solid; mp: 105.1 °C; ^{1}H NMR (400 MHz; DMSO-d_6) δ 6.24 (s, 1H, >C═CH), 7.11−7.13 (m, 2H, Ar), 7.19−7.20 (m, 2H, Ar), 7.20−7.32 (m, 3H, Ar), 7.32−7.35 (m, 2H, Ar), 8.02 (s, 1H, NH exch).

*3.1.3. General Procedure for the Synthesis of Methyl 2-((3,4-Diphenylthiazol-2(3H)-ylidene)amino)acetate (**8a−d, 8j, 8l,** and **8m**).* Compound **7a** (750 mg, 2 mmol) was placed in a round bottom flask in dry acetone (10 mL) under nitrogen. Once the clear solution was formed, 2.5 mmol (345 mg) of potassium carbonate was placed in a reaction vessel on continuous stirring at room temperature. After 30 min of incubation of the reaction mixture, 2.2 mmol (306 mg) of methyl 2-bromoacetate was added to the reaction mixture and stirring continued at 80 °C. Reaction progress was monitored by TLC. Once the reaction was completed, the solvent was removed under reduced pressure. The solid residue so obtained was quenched with ice cold aqueous solution of sodium bicarbonate. The so-obtained solid was purified by column chromatography to give the pure product.

*3.1.3.1. Methyl 2-((3,4-Diphenylthiazol-2(3H)-ylidene)-amino)acetate (**8a**).* The yield was 85%; solid; mp: 132.3 °C; ^{1}H NMR (400 MHz; DMSO-d_6) δ 2.74 (s, 3H, CH_3), 3.57 (s, 2H, CH_2), 6.50 (s, 1H, >C═CH), 7.25−7.27 (m, 2H, Ar), 7.36−7.38 (m, 5H, Ar), 7.45−7.46 (m, 3H, Ar). ^{13}C NMR

https://doi.org/10.1021/acsomega.2c07569
ACS Omega 2023, 8, 17552−17562

(400 MHz; DMSO-d_6) δ 170.44, 160.92, 146.10, 137.71, 133.56, 132.17, 130.50, 130.90, 129.84, 129.32, 129.15, 129.03, 128.58, 128.56, 125.80, 99.05, 55.30, 52.01. MS (m/z) 325.09. Elemental Analysis: (calculated), found, (C, 66.64%; H, 4.97%; N, 8.64%; S, 9.88%) C, 66.63%; H, 4.95%; N, 8.61%; S, 9.87%.

Other compounds were prepared by following a similar procedure.

*3.1.3.2. Methyl 2-((3-(2-Methoxyphenyl)-4-phenylthiazol-2(3H)-ylidene)amino)acetate (**8b**).* The elution solvent was hexane/ethyl acetate (8:2); yield 82%; solid; mp: 105.3 °C; ^{1}H NMR (400 MHz; DMSO-d_6) δ 3.53 (s, 3H, OCH_3), 3.61 (s, 3H, OCH_3), 3.77−3.89 (q, 2H, CH_2), 6.39 (s, 1H, >C═CH), 6.92−6.96 (m, 2H, Ar), 7.11−7.13 (m, 2H, Ar), 7.19−7.28 (m, 5H, Ar). ^{13}C NMR (400 MHz; DMSO-d_6) δ 171.06, 162.60, 140.32, 131.75, 131.63, 130.21, 128.85, 128.43, 128.20, 127.10, 121.01, 113.21, 96.63, 56.02, 55.46, 52.01. MS (m/z) 345.61 $(M + H)^+$. Elemental Analysis: (calculated), found, (C, 66.64%; H, 4.97%; N, 8.64%; S, 9.88%), C, 66.61%; H, 4.95%; N, 8.63%; 9.85%.

*3.1.3.3. Methyl 2-((3-(2-Nitrophenyl)-4-phenylthiazol-2(3H)-ylidene)amino)acetae (**8c**).* The elution solvent was hexane/ethyl acetate (8:2); yield 78%; solid; mp: 97.4 °C; ^{1}H NMR (400 MHz; DMSO-d_6) δ 3.55 (s, 3H, OCH_3), 3.76 (s, 2H, CH_2), 6.54 (s, 1H, >C═CH), 7.15−7.17 (m, 2H, Ar), 7.20−7.23 (m, 4H, Ar), 7.49−7.52 (td, 1H, Ar), 7.57−7.60 (m, 1H, Ar), 7.98−8.00 (m, 1H, Ar).^{13}C NMR (400 MHz; DMSO-d_6) δ 170.95, 155.49, 140.85, 138.71, 134.56, 132.17, 131.50, 130.90, 129.86, 129.34, 129.05, 129.03, 128.59, 128.57, 125.70, 99.07, 55.31, 52.02. MS (m/z) 371.61$(M + H)^+$. Elemental Analysis: (calculated), found, (C, 58.53%; H, 4.09%; N, 11.38%; S, 8.68%), C, 58.51%; H, 4.07%; N, 11.37%; S, 8.68%.

*3.1.3.4. Methyl 2-((4-Phenyl-3-(o-tolyl)thiazol-2(3H)-ylidene)amino)acetate (**8d**).* The elution solvent was hexane/ethyl acetate (8:2); yield 78%; solid; mp: 98.2 °C; ^{1}H NMR (400 MHz; DMSO-d_6) δ 2.26 (s, 3H, CH_3), 3.62 (s, 3H, OCH_3), 3.85 (s, 2H, CH_2), 6.46 (s, 1H, >C═CH), 7.01−7.03 (m, 3H, Ar), 7.10−7.16 (m, 4H, Ar), 7.23−7.25 (m, 3H, Ar). ^{13}C NMR (400 MHz; DMSO-d_6) δ 171.04, 161.61, 141.31, 136.34, 134.97, 130.93, 129.82, 129.32, 128.94, 128.86, 128.73, 97.93, 55.67, 52.19, 21.05. MS (m/z) 339.59$(M + H)^+$. Elemental Analysis: (calculated), found, (C, 67.43%; H, 5.36%; N, 8.28%; S, 9.47%), C, 67.41%; H, 5.34%; N, 8.27%; S, 9.45%.

*3.1.3.5. Methyl 2-((3-(4-Methoxyphenyl)-4-phenylthiazol-2(3H)-ylidene)amino)acetate (**8j**).* The elution solvent was hexane/ethyl acetate (8:2); yield 80%; solid; mp: 96.3 °C; ^{1}H NMR (400 MHz; DMSO-d_6) δ 3.68 (s, 3H, OCH_3), 3.78 (s, 3H, OCH_3), 3.92 (s, 2H, CH_2), 6.50 (s, 1H, >C═CH), 6.91−6.93 (m, 2H, Ar), 7.12−7.14 (m, 2H, Ar), 7.21−7.22 (m, 2H, Ar), 7.30−7.31 (m, 3H, Ar). ^{13}C NMR (400 MHz; DMSO-d_6) δ 171.96, 162.66, 158.59, 140.34, 131.80, 131.09, 130.64, 128.83, 128.74, 128.66, 114.42, 97.44, 55.74, 55.56, 52.04. MS (m/z) 355.62 $(M + H)^+$. Elemental Analysis: (calculated), found, (C, 64.39%; H, 5.12%; N, 7.90%; S, 9.05%), C, 64.37%; H, 5.11%; N, 7.90%; S, 9.03%.

*3.1.3.6. Methyl 2-((4-Phenyl-3-(p-tolyl)thiazol-2(3H)-ylidene)amino)acetate (**8l**).* The elution solvent was hexane/ethyl acetate (8:2); yield 75%; solid; mp: 99.2 °C; ^{1}H NMR (400 MHz; DMSO-d_6) δ 2.31 (s, 3H, CH_3), 3.67 (s, 3H, OCH_3), 3.91 (s, 2H, CH_2), 6.51 (s, 1H, >C═CH), 7.07−7.09 (m, 2H, Ar), 7.16−7.21 (m, 4H, Ar), 7.28−7.29 (m, 3H, Ar). ^{13}C NMR (400 MHz; DMSO-d_6) δ 171.06, 162.60, 140.32, 137.35, 135.98, 131.93, 129.85, 129.36, 128.96, 128.87, 128.72, 97.92, 55.68, 52.18 21.04. MS (m/z) 339.55 $(M + H)^+$. Elemental Analysis: (calculated), found, (C, 67.43%; H, 5.36%; N, 8.28%; S, 9.47%), C, 67.41%; H, 5.33%; N, 8.27%; S, 9.46%.

*3.1.3.7. Methyl 2-((3-(4-Chlorophenyl)-4-phenylthiazol-2(3H)-ylidene)amino)acetate (**8m**).* The elution solvent was hexane/ethyl acetate (8:2); yield 75%; solid; mp: 98.3 °C; ^{1}H NMR (400 MHz; DMSO-d_6) δ 3.58 (s, 3H, CH_3), 3.83 (s, 2H, CH_2), 6.47 (s, 1H, >C═CH), 7.10−7.12 (m, 2H, Ar), 7.13−7.15 (m, 2H, Ar), 7.22−7.23 (m, 3H, Ar), 7.32−7.35 (m, 2H, Ar). ^{13}C NMR (400 MHz; DMSO-d_6) δ 170.45, 160.93, 145.10, 138.71, 134.56, 132.17, 131.50, 130.90, 129.86, 129.34, 129.05, 129.03, 128.59, 128.57, 125.70, 99.07, 55.31, 52.02. MS (m/z) 359.57$(M + H)^+$. Elemental Analysis: (calculated), found, (C, 60.25%; H, 4.21%; N, 7.81%; S, 8.94%), C, 60.23%; H, 4.19%; N, 7.79%; S, 8.92%.

■ ASSOCIATED CONTENT

Supporting Information

The Supporting Information is available free of charge at https://pubs.acs.org/doi/10.1021/acsomega.2c07569.

Molecular docking; *in vitro* cytotoxicity of the compounds; *in silico* ADMET profiling of the compounds; NMR spectra of compounds, mass spectrograms, and HPLC analysis of the compounds (PDF)

■ AUTHOR INFORMATION

Corresponding Authors

Vinit Kumar − *Amity Institute of Molecular Medicine and Stem Cell Research, Amity University, Noida 201303 Uttar Pradesh, India*; Email: vinitiitr@gmail.com, vkumar25@amity.edu

Reshma Rani − *Drug Discovery, Jubilant Biosys, Greater Noida 201306, India*; orcid.org/0000-0003-4937-0689; Email: reshudcy@gmail.com

Authors

Dolly Sharma − *Amity Institute of Biotechnology, Amity University, Noida 201303 Uttar Pradesh, India; Amity Institute of Molecular Medicine and Stem Cell Research, Amity University, Noida 201303 Uttar Pradesh, India*

Mamta Singh − *Amity Institute of Molecular Medicine and Stem Cell Research, Amity University, Noida 201303 Uttar Pradesh, India*

Jayadev Joshi − *Genomic Medicine Institute, Lerner Research Institute, Cleveland Clinic, Cleveland, Ohio 44195, United States*

Manoj Garg − *Amity Institute of Molecular Medicine and Stem Cell Research, Amity University, Noida 201303 Uttar Pradesh, India*

Vidhi Chaudhary − *India Institute of Technology Patna, Patna 801106, India*

Daniel Blankenberg − *Genomic Medicine Institute, Lerner Research Institute, Cleveland Clinic, Cleveland, Ohio 44195, United States*

Sudhir Chandna − *Institute of Nuclear Medicine & Allied Science, Defense Research Development Organization, Delhi 110054, India*

Complete contact information is available at: https://pubs.acs.org/10.1021/acsomega.2c07569

https://doi.org/10.1021/acsomega.2c07569
ACS Omega 2023, 8, 17552−17562

Author Contributions

R.R. and V.K. performed the conceptualization, supervision, investigation, data analysis, and writing. D.S. conducted the synthesis, data curation, data analysis, and writing. M.S. completed the *in vitro* studies. V.C. was in charge of the NMR. J.S. and D.B. took over the molecular docking. M.G. took charge of the anticancer activities in pancreatic cancer cells. S.C. executed the *in vitro* studies. All authors approved the submitted version.

Funding

This work was funded by a SERB grant (ECR/2017/000548) to R.R.

Notes

The authors declare no competing financial interest.

■ ACKNOWLEDGMENTS

D.S., M.S., V.K., and R.R. thank Amity University UP India for providing necessary support. R.R. also acknowledges the support of SERB to carry out this work.

■ REFERENCES

(1) Hanahan, D.; Weinberg, R. A. Hallmarks of cancer: The next generation. *Cell* **2011**, *144*, 646−674.
(2) Martinez-Outschoorn, U. E.; Peiris-Pagés, M.; Pestell, R. G.; Sotgia, F.; Lisanti, M. P. Cancer metabolism: A therapeutic perspective. *Nat. Rev. Clin. Oncol.* **2017**, *14*, 11−31.
(3) Kumar, V.; Rani, R. Lactate dehydrogenase enzyme: An old enzyme but new viable target offers new hope in cancer therapeutics. *Lactate Dehydrogenase (LDH): Biochemistry, Function and Clinical Significance 1*.
(4) Sharma, D.; Singh, M.; Rani, R. Role of LDH in tumor glycolysis: Regulation of LDHA by small molecules for cancer therapeutics. *Semin. Cancer Biol.* **2022**, *87*, 184−195.
(5) Sharma, D.; Singh, M.; Gupta, R.; Kumar, V.; Kumar, V.; Rani, R. Intervention on lactate in cancer: A promising approach for the development of cancer therapeutics. *Adv. Cancer Biol.: Metastasis* **2022**, *5*, 100058.
(6) Intlekofer, A. M.; Finley, L. W. S. Metabolic signatures of cancer cells and stem cells. *Nat. Metab.* **2019**, *1*, 177−188.
(7) Menendez, J. A.; Alarcón, T. Metabostemness: A new cancer hallmark. *Front. Oncol.* **2014**, *4*, 262.
(8) Jagust, P.; De Luxán-Delgado, B.; Parejo-Alonso, B.; Sancho, P. Metabolism-based therapeutic strategies targeting cancer stem cells. *Front. Pharmacol.* **2019**, *10*, 203.
(9) Kumar, V.; Rani, R. Selective inhibitors of human lactate dehydrogenase A to fight against metabolic cancer: a patent landscape. *Pharm. Pat. Anal.* **2020**, *9*, 155−157.
(10) Singh, M.; Afonso, J.; Sharma, D.; Gupta, R.; Kumar, V.; Rani, R.; Baltazar, F.; Kumar, V. Targeting Monocarboxylate Transporters (MCTs) in cancer: How close are we to the clinics? *Semin. Cancer Biol.* **2023**, *90*, 1−14.
(11) Fakhri, S.; Moradi, S. Z.; Farzaei, M. H.; Bishayee, A. Modulation of dysregulated cancer metabolism by plant secondary metabolites: A mechanistic review. *Semin. Cancer Biol.* **2022**, *80*, 276−305.
(12) Rani, R.; Kumar, V. Recent Update on Human Lactate Dehydrogenase Enzyme 5 (hLDH5) Inhibitors: A Promising Approach for Cancer Chemotherapy. *J. Med. Chem.* **2016**, *59*, 487−496.
(13) Kumar, A.; Singh, M.; Sharma, D.; Kumar, V.; Rani, R. Tumor Metabolism: Focused on Tumor Glycolysis, Progress, and Prospects in Cancer Therapy. *Burger's Medicinal Chemistry and Drug Discovery*; Wiley, 2021; pp 1−33.
(14) Le, A.; Cooper, C. R.; Gouw, A. M.; Dinavahi, R.; Maitra, A.; Deck, L. M.; Royer, R. E.; Vander Jagt, D. L.; Semenza, G. L.; Dang, C. V. Inhibition of lactate dehydrogenase A induces oxidative stress and inhibits tumor progression. *Proc. Natl. Acad. Sci. U.S.A.* **2010**, *107*, 2037−2042.
(15) Rani, R.; Kumar, V. When will small molecule lactate dehydrogenase inhibitors realize their potential in the cancer clinic? *Fut. Med. Chem.* **2017**, *9*, 1113−1115.
(16) Maftouh, M.; Avan, A.; Sciarrillo, R.; Granchi, C.; Leon, L. G.; Rani, R.; Funel, N.; Smid, K.; Honeywell, R.; Boggi, U.; et al. Synergistic interaction of novel lactate dehydrogenase inhibitors with gemcitabine against pancreatic cancer cells in hypoxia. *Br. J. Cancer* **2014**, *110*, 172−182.
(17) Andrews, B. A.; Dyer, R. B. Small molecule cores demonstrate non-competitive inhibition of lactate dehydrogenase. *Med. Chem. Commun.* **2018**, *9*, 1369−1376.
(18) Friberg, A.; Rehwinkel, H.; Nguyen, D.; Pütter, V.; Quanz, M.; Weiske, J.; Eberspächer, U.; Heisler, I.; Langer, G. Structural Evidence for Isoform-Selective Allosteric Inhibition of Lactate Dehydrogenase A. *ACS Omega* **2020**, *5*, 13034−13041.
(19) Li, X.-M.; Xiao, W.-H.; Zhao, H.-X. Discovery of potent human lactate dehydrogenase A (LDHA) inhibitors with antiproliferative activity against lung cancer cells: virtual screening and biological evaluation. *Med. Chem. Commun.* **2017**, *8*, 599−605.
(20) Jabalia, N.; Kumar, A.; Kumar, V.; Rani, R. In Silico Approach in Drug Design and Drug Discovery: An Update. *Innovations and Implementations of Computer Aided Drug Discovery Strategies in Rational Drug Design*; Springer, 2021; pp 245−271.
(21) Singh, M.; Gupta, R.; Comez, L.; Paciaroni, A.; Rani, R.; Kumar, V. BCL2 G quadruplex-binding small molecules: Current status and prospects for the development of next-generation anticancer therapeutics. *Drug Discov. Today* **2022**, *27*, 2551−2561.
(22) Morigi, R.; Locatelli, A.; Leoni, A.; Rambaldi, M. Recent Patents on Thiazole Derivatives Endowed with Antitumor Activity. *Recent Pat. Anticancer Drug Discov.* **2015**, *10*, 280−297.
(23) Sharma, P. C.; Bansal, K. K.; Sharma, A.; Sharma, D.; Deep, A. Thiazole-containing compounds as therapeutic targets for cancer therapy. *Eur. J. Med. Chem.* **2020**, *188*, 112016.
(24) Kaplancikli, Z. A.; Altıntop, M. D.; Atli, O.; Sever, B.; Baysal, M.; Temel, H. E.; Demirci, F.; Ozdemir, A. Synthesis and Evaluation of A New Series of Thiazole Derivatives as Potential Antitumor Agents and MMP Inhibitors. *Anticancer Agents Med. Chem.* **2017**, *17*, 674−681.
(25) Farghaly, T. A.; Abbas, E. M. H.; Al-Soliemy, A. M.; Sabour, R.; Shaaban, M. R. Novel sulfonyl thiazolyl-hydrazone derivatives as EGFR inhibitors: Design, synthesis, biological evaluation and molecular docking studies. *Bioorg. Chem.* **2022**, *121*, 105684.
(26) Gümüş, M.; Yakan, M.; Koca, I. Recent advances of thiazole hybrids in biological applications. *Future Med. Chem.* **2019**, *11*, 1979−1998.
(27) Aoyama, T.; Murata, S.; Arai, I.; Araki, N.; Takido, T.; Suzuki, Y.; Kodomari, M. One pot synthesis using supported reagents system KSCN/SiO2−RNH3OAc/Al2O3: synthesis of 2-aminothiazoles and N-allylthioureas. *Tetrahedron* **2006**, *62*, 3201−3213.
(28) Sondhi, S. M.; Rani, R.; Gupta, P. P.; Agrawal, S. K.; Saxena, A. K. Synthesis, anticancer, and anti-inflammatory activity evaluation of methanesulfonamide and amidine derivatives of 3,4-diaryl-2-imino-4-thiazolines. *Mol. Divers.* **2009**, *13*, 357−366.
(29) Monks, A.; Scudiero, D.; Skehan, P.; Shoemaker, R.; Paull, K.; Vistica, D.; Hose, C.; Langley, J.; Cronise, P.; Vaigro-Wolff, A.; et al. Feasibility of a high-flux anticancer drug screen using a diverse panel of cultured human tumor cell lines. *J. Natl. Cancer Inst.* **1991**, *83*, 757−766.
(30) Pascale, F.; Bedouet, L.; Baylatry, M.; Namur, J.; Laurent, A. Comparative Chemosensitivity of VX2 and HCC Cell Lines to Drugs Used in TACE. *Anticancer Res.* **2015**, *35*, 6497−6503.
(31) Benyettou, F.; Fahs, H.; Elkharrag, R.; Bilbeisi, R. A.; Asma, B.; Rezgui, R.; Motte, L.; Magzoub, M.; Brandel, J.; Olsen, J. C.; et al. Selective growth inhibition of cancer cells with doxorubicin-loaded CB[7]-modified iron-oxide nanoparticles. *RSC Adv.* **2017**, *7*, 23827−23834.

https://doi.org/10.1021/acsomega.2c07569
ACS Omega 2023, 8, 17552−17562

(32) https://www.cancerrxgene.org/compound/Doxorubicin/133/overview/ic50 (accessed March 02, 2023).
(33) Lipinski, C. A.; Lombardo, F.; Dominy, B. W.; Feeney, P. J. Experimental and computational approaches to estimate solubility and permeability in drug discovery and development settings. *Adv. Drug Deliv. Rev.* **1997**, *23*, 3−25.

https://doi.org/10.1021/acsomega.2c07569
ACS Omega 2023, 8, 17552−17562